JOURNAL OF MATERIALS SCIENCE **37** (2002) 1005–1017

Mechanical characterization of soft materials using high speed photography and split hopkinson pressure bar technique

A. SHARMA, A. SHUKLA
Department of Mechanical Engineering, University of Rhode Island, Kingston, RI 02881, USA
E-mail: sharmaa@egr.uri.edu; shuklaa@egr.uri.edu

R. A. PROSSER
US Army Natick, Soldier System Center, Natick, MA 01760, USA
E-mail: Robert.Prosser@natick.army.mil

High-speed photography in conjunction with the viscoelastic Split Hopkinson Pressure Bar (SHPB) technique was used to study soft material behavior under dynamic loading conditions. The real-time strains recorded using high speed photography were also used for validating the existing viscoelastic SHPB model. Polyurethane, sculpturing clay, sorbothane and bologna were tested as examples of soft materials. The dynamic compressive strength of clay increased by 4 orders of magnitude compared to the static compressive strength. The dynamic strength of sorbothane increased by 3 orders of magnitude compared to the manufacturer specified static values. Only dynamic experiments, between strain rates of 2700 and 3700/sec, were performed on bologna. All the four materials showed very high strain-rate dependence. The tested materials showed similar stress-strain plots. Clay, Sorbothane and Bologna were very compliant up to 30 to 35% strains followed by a stiffer region where the stresses increased rapidly to the maximum values. The specimens were in stress equilibrium for significant time durations and specimen peak stresses where achieved during this period.

1. Introduction

Low mechanical impedance materials are increasingly being used in applications subjected to high strain rates and deformations. Examples of such applications are crushable foams in vehicle interiors for passenger protection during crashes, high-speed plastic forming processes, shock absorption applications in the electronic packaging and sporting goods industry and for the design of high performance body armor.

For the case of a bullet stopped by a typical hard armor system some of the original kinetic energy of the bullet will be dissipated by destruction of the ceramic front plate, however, a significant proportion will result in a stress wave being generated in the material of the armor, which in turn can be coupled to the body. This stress wave can travel at velocities considerably greater than the velocity of the bullet and is available to cause damage to the body, as in the case of the shock wave in blast injuries Bell [1]. Injuries associated with explosive blast primarily affect the air containing organs, injury to the lung being the most devastating. The lung consists of numerous air sacs, excitation can cause these sacs to resonate leading to large shear stresses within the tissues surrounding the sac and if the shear stress exceeds the elastic limit of the tissue then the tissue will rupture, Cooper [2]. The maximum stress and strain level the tissue can withstand before rupturing depends on the constitutive behavior of tissues under dynamic loading.

Accurate mechanical property data at high strain rates would be a fundamental component of any realistic numerical simulation of soft tissue injuries. In order to gain insight into how these tissues behave in injurious loading conditions, the response of these materials must be quantified at high loading rates. Three compliant materials; Sorbothane, Sculpturing clay *Roma Plastilina No. 2* and Bologna were chosen for this study. Polyurethane is one of the softest materials that has been tested using the conventional steel SHPB setups. This material was chosen to validate the viscoelastic SHPB setup developed with existing literature. Sorbothane has been used for shock absorption applications in the sporting goods industry. Sculpturing clay is believed to have dynamic properties similar to human lung tissue and finally bologna was tested as an example of soft biological material.

Sorbothane is of special interest because it is a dilatant material. Its viscosity increases as the shear rate increases. At high shear rates these materials can become quite hard. Sorbothane may be useful as back-up material for flexible armor. A layer would be positioned between the human body and the ceramic armor, and thereby provide a soft surface that would better conform to the human body making the armor much more

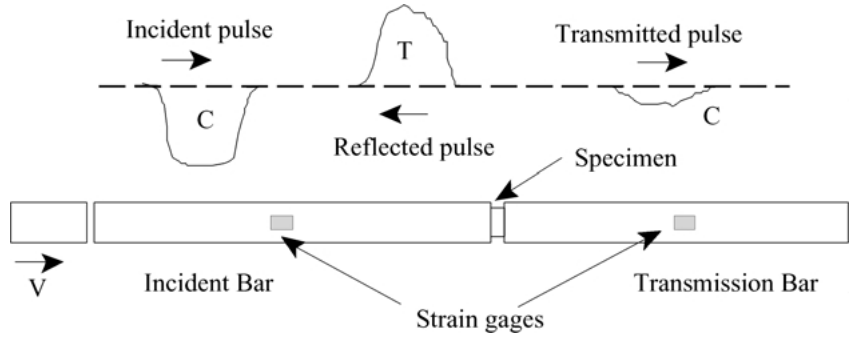

Figure 1 Schematic of a SHPB setup.

comfortable. When struck by a projectile or ceramic shards, however, high strain rates would ensue causing the material to stiffen and better inhibit projectile penetration. Also, the sorbothane layer would help in reducing behind the armor effect by attenuating the magnitude of shock waves entering the human body. The effectiveness of this material/concept is yet to be determined.

Dynamic experiments were conducted at strain-rates between 2400 to 3700/s using a viscoelastic SHPB setup. Along with the viscoelastic SHPB, real-time measurements of strain and displacements were obtained using high-speed photography and compared with the viscoelastic analysis results to get more physical insight into the behavior of soft materials under dynamic loading conditions. The average axial and transverse specimen strains were measured using high-speed photography techniques. There was a good match between the instantaneous transverse specimen dimensions recorded using the high-speed camera and the theoretically predicted instantaneous diameters based on mass conservation and specimen material incompressibility.

2. Viscoelastic SHPB theoretical models

The Split Hopkinson Pressure Bar (SHPB) technique, developed by Kolsky [3], has been widely used in studying the constitutive behavior of materials under dynamic compressive loads, Fig 1. In testing soft materials using conventional SHPB the transmitted signal has very small amplitude, resulting in a low transmitted signal to noise ratio. The transmitted signal is used in calculating stresses in the specimen. The low amplitude of transmitted signal increases the level of uncertainty, thus making it difficult to obtain reliable stress-strain responses. The low amplitude of transmitted signals is due to the high impedance mismatch between the hard SHPB pressure bars (usually steel) and the soft test material. Due to low impedance of the test material most of the incident stress pulse will be reflected back into the incident bar, yielding a small amplitude transmitted signal.

Conventional SHPB analysis assumes uni-axial loading of the specimen. If the amplitude of loading pulse exceeds the dynamic strength of test material within its rise time, specimen would deform non-homogeneously before failure. Thus, the specimen will deform plastically near the incident end, whereas deformation would be small at the other end, resulting in a non-equilibrium stress state. This stress state is due to the slower wave velocities in low-impedance materials. To reach equilibrium in the specimen, the loading pulse should reverberate at least three times in the specimen [4]. Gray and Blumenthal have also discussed in detail specimen stress-state equilibrium, sample size and strain-rates effects using experimental as well as numerical techniques, [5, 6]. Thus, suitable modifications are essential to use the SHPB technique for accurately measuring the dynamic mechanical response of compliant materials.

Forrestal *et al.* [7] have developed a SHPB setup using hollow aluminum pressure bars for increasing the transmitted signal by decreasing the pressure-bar/specimen area ratio. Use of pressure bars having lower modulus of elasticity like polycarbonate, PMMA, etc. reduces the impedance mismatch between the test specimen and pressure bars, thus giving a higher amplitude transmitted strain signal. However, if viscoelastic bars are used the conventional SHPB analysis cannot be used. Due to attenuation and dispersion of stress pulse in the polymeric bars, the strain signals recorded at the strain gage locations, cannot be directly used to find stresses and particle velocities at the specimen-bar interface. Therefore, stress-strain relations need to be developed which take into account the viscoelastic behavior of polymeric pressure bars.

Wang *et al.* [8] have developed a SHPB analysis method based on the characteristics theory of wave propagation and the Zhu-Wang-Tang (ZWT) viscoelastic constitutive model, Fig. 2. Experimental investigations of plastics have shown that their nonlinear viscoelastic behavior can be modeled by the ZWT Equation 1:

$$\sigma = E_0\varepsilon + \alpha\varepsilon^2 + \beta\varepsilon^3 + E_1\int_0^t \varepsilon(\tau)\,\mathrm{e}^{-\left(\frac{t-\tau}{\theta_1}\right)}\,\mathrm{d}\tau + E_2\int_0^t \varepsilon(\tau)\,\mathrm{e}^{-\left(\frac{t-\tau}{\theta_2}\right)}\,\mathrm{d}\tau \quad (1)$$

where the first three terms describe the nonlinear response; the first integral term describes the viscoelastic response at low strain rates; and the second integral term describes the viscoelastic response for high strain rates.

For the high strain rate conditions of SHPB testing, the low frequency Maxwell element will behave like

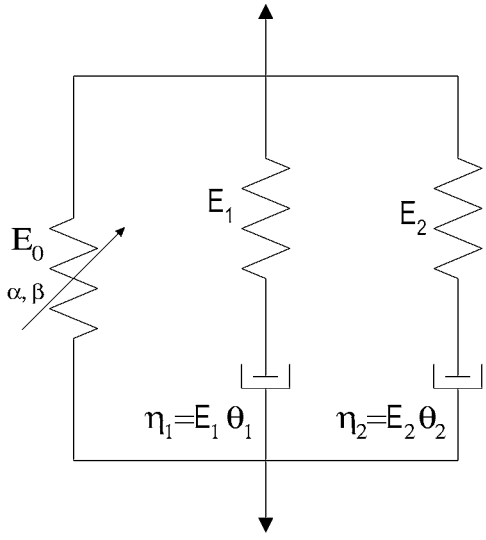

Figure 2 Model corresponding to Zhu-Wang-Tang constitutive equation.

an elastic solid of stiffness E_1. Also, since the deformations in the pressure bars are small (0.0014 m), the second and third terms of Equation 1 may be neglected. Thus, the constitutive equation for the SHPB setup is given as

$$\sigma = (E_0 + E_1)\varepsilon + E_2 \int_0^t \varepsilon(\tau)\, \mathrm{e}^{-\left(\frac{t-\tau}{\theta_2}\right)} \mathrm{d}\tau \qquad (2)$$

Combining Equation 2 with the equation of motion and continuity equations for thin bars, a solution to the wave equation for viscoelastic bars can be obtained in terms of the particle displacements.

The elastic wave velocity C_v in the pressure bars and the wave attenuation constant α_a can be determined experimentally from a single bar impact test. The remaining viscoelastic pressure bar constants E_0, E_1 and θ_2 can be determined from the knowledge of C_v, α_a and static testing results. Using the material constitutive equations and the strain-time histories (recorded at the strain gage locations), we can then find the stresses and particle velocities at the specimen-bar interface by time shifting of the recorded strain signals.

Wang *et al*. did not consider geometric effects in their analysis. Zhao *et al.* [9] generalized the Pochhammer and Chree equation for an elastic cylindrical bar to the case of viscoelastic bars. These modified viscoelastic equations are solved numerically and the results are used to take into account the wave dispersion and attenuation in polymeric bars. Sawas *et al.* [10] have proposed a method that uses an experimentally identified auxiliary function to establish relaxation and creep functions. This technique requires priori knowledge of the constitutive model of the viscoelastic bars.

Bacon [11] has proposed a method to experimentally determine the propagation coefficients of a viscoelastic bar, and apply these coefficients to obtain the force and particle velocities at the specimen-bar interface. In this method, the one-dimensional wave equation for an axially impacted long cylindrical bar is written in the Fourier domain. The viscoelastic bar material can then be described by a linear stress-strain equation involving a complex modulus. This approach greatly simplifies the one-dimensional equation of axial motion in viscoelastic bars, Equation 3.

$$\left(\frac{\partial^2}{\partial x^2} - \gamma^2\right)\tilde{\varepsilon}(x, \omega) = 0 \qquad (3)$$

The general solution of Equation 3 is given by

$$\tilde{\varepsilon}(x, \omega) = \tilde{P}(\omega)\, \mathrm{e}^{-\gamma x} + \tilde{N}(\omega)\, \mathrm{e}^{\gamma x} \qquad (4)$$

where $\tilde{\varepsilon}(x, \omega)$ denotes the Fourier transform of strain, the functions $\tilde{P}(\omega)$ and $\tilde{N}(\omega)$ define the Fourier transforms of the strains at the strain gage locations due to the waves traveling in the directions of increasing and decreasing x, respectively. $\gamma = \gamma(\omega)$ is the propagation coefficient, which depends on the complex Young's modulus of the material and the angular frequency (ω).

From Equation 4 we can find the Fourier transforms of the axial particle velocity $\tilde{v}(x, \omega)$ and the normal force $\tilde{F}(x, \omega)$ at any cross section x. The propagation coefficient can be determined experimentally, by impacting one bar with a projectile and recording the incident $\varepsilon_1(t)$ and the first reflected pulse $\varepsilon_2(t)$. Using the knowledge of the forces and particle velocities at the specimen-bar interface we can find the stress and strains in the specimen.

Fourney *et al.* [12] have used a 3-parameter Kelvin model to represent the viscoelastic pressure bars, Fig. 3. The constitutive equation for the 3-parameter Kelvin model is:

$$\frac{\partial \varepsilon}{\partial t} + \frac{\varepsilon}{\theta_1} - \frac{(E_0 + E_1)}{E_0 E_1 \theta_1}\sigma - \frac{1}{E_0}\frac{\partial \sigma}{\partial t} = 0 \qquad (5)$$

For the case of quasi-static loading conditions, the time dependent terms disappear and Equation 5 reduces to

$$\sigma = \frac{E_0 E_1}{E_0 + E_1}\varepsilon \equiv E'\varepsilon \qquad (6)$$

$E' \equiv \frac{E_0 E_1}{E_0 + E_1}$ is the quasi-static modulus of the viscoelastic material. Combining Equation 5 with the equation of motion and continuity equations, the 1-D wave equation for viscoelastic bars can be written in the differential form as

$$\rho\frac{\partial^3 u}{\partial t^3} + \rho\frac{(E_0 + E_1)}{E_1\theta_1}\frac{\partial^2 u}{\partial t^2} = E_0\frac{\partial^3 u}{\partial t \partial x^2} + \frac{E_0}{\theta_1}\frac{\partial^2 u}{\partial x^2} \qquad (7)$$

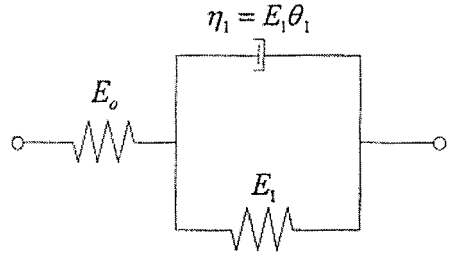

Figure 3 3 Parameter Kelvin model.

The solution to Equation 7 is

$$u(x,t) = A\,\mathrm{e}^{\pm\alpha_a x}\,\mathrm{e}^{i(wt\pm kx)} \tag{8}$$

The minus sign corresponds to the waves propagating in positive x-direction, while plus sign corresponds to waves traveling in negative x-direction. ω is the radial frequency, k is the wave number and α is the attenuation constant.

The incident, reflected and transmitted waves are determined from the signals measured at the strain gage locations by using the method of characteristics, Graff [13]. The characteristics method is well known for the one-dimensional longitudinal wave propagation in thin bars. Using the method of characteristics, the relations between the elastic wave velocity C_v, the attenuation constant α and the three material modeling parameters are

$$C_v^2 = \frac{\omega^2}{k^2} = \frac{E_1}{\rho} \tag{9}$$

$$\alpha = \frac{E_0}{2\theta_1 C_v E_1} \tag{10}$$

C_v and α can be determined experimentally by measuring the elastic wave velocity and the logarithmic decrement of the stress pulse amplitude from a single bar impact test. The static compressive modulus E' of the pressure bar material is related to the two modulii E_0, E_1 through the relation

$$E' = \frac{E_0 E_1}{E_0 + E_1} \tag{11}$$

θ_1 can then be determined from Equation 10.

Once the pressure bar materials have been characterized, the method of characteristics can be used to determine the particle velocities and stresses at the specimen-bar interface from the strains recorded at the strain gage locations. The stress at some distance Δx downstream of the strain wave is converted into the stress at time $\Delta t = \frac{\Delta x}{C_v}$ later,

$$\sigma_N = \sigma_{N-1} + E_0(\varepsilon_N - \varepsilon_{N-1}) - \frac{(\sigma_{N-1} - E'\varepsilon_{N-1})}{E'\theta_1} E_0 \Delta t \tag{12}$$

N denotes the current step and $N-1$ denotes the previous step. The initial condition at the free end of the bar is $\varepsilon(0) = \sigma(0) = v(0) = 0$. The velocity at the interface can be calculated as

$$v_N = v_{N-1} \pm \frac{(\sigma_N - \sigma_{N-1})}{\rho C_v} \pm \frac{(\sigma_{N-1} - E'\varepsilon_{N-1})}{E'\theta_1} C_v \Delta t \tag{13}$$

Once the stresses and particle velocities at the specimen-bar interface are determined, the specimen stresses, strains and strain-rate can be calculated from the basic SHPB equations,

$$\sigma_s(t) = \frac{A_b}{A_{si}}(\sigma_i + \sigma_r + \sigma_t) \tag{14a}$$

$$\dot{\varepsilon}(t) = \frac{v_2(t) - v_1(t)}{l_{si}} = \frac{v_t(t) - v_i(t) - v_r(t)}{l_{si}} \tag{14b}$$

$$\varepsilon = \int_0^t \dot{\varepsilon}(t)\,\mathrm{d}t = \frac{1}{l_{si}} \int_0^t (v_t(t) - v_i(t) - v_r(t))\,\mathrm{d}t \tag{14c}$$

where the subscripts t, i and r denote the corresponding quantities of transmitted, incident and reflected waves respectively. A_{si} is the instantaneous cross-sectional area of the specimen and A_b is the pressure bar cross-sectional area. l_{si} represents the instantaneous specimen length.

3. Experimental procedure

The pressure bars were made from polycarbonate (distributed by Modern Plastics under the trade name of Lexan) having a diameter of 19.05 mm and length of 1.24 m each. Three different length projectiles, 152 mm, 254 mm and 356 mm having a cross-section of 12.7 mm, were used in this study. The projectiles were made from PMMA manufactured by Modern Plastics. All the projectiles were fired at 210 kPa gas gun firing pressure. Various pulse shapers were used to increase the rise time of the pulses and to protect the pressure bars from permanent deformation. The bar properties are given in Table I. These were obtained from a single bar impact test Equations 9–11.

The specimen diameters were chosen such that the cross sectional area of the specimen would not exceed the cross sectional area of the pressure bars at any time during the test. The polyurethane specimen was a disc of 9.5 mm diameter and 3.3 mm length. The polyurethane specimens were punched out of a polyurethane cast sheet. The clay specimen was a disc of diameter 9.5 mm and 3.3 mm length. The specimens were made by compaction in a mold. The sorbothane specimen was a disc of diameter 8.1 mm and length 3.2 mm. Specimens were punched out of a 3.2 mm thick sorbothane sheet hardened by cooling to dry ice temperatures. The bologna specimens were punched out of a 3.3 mm thick bologna slice. The specimen diameter was 9.5 mm.

A thin layer of silicon oil based lubricant was applied to the two bar ends to minimize friction between the specimen and pressure bars. The specimen was sandwiched between the incident and transmitted bars.

TABLE I Polycarbonate pressure bar material properties

$\alpha =$	0.0673	(/m)
$c =$	1420	m/s
$E_0 =$	2.42	GPa
$E_1 =$	71.1	GPa
$E' =$	2.34	GPa
$\theta_1 =$	178	μsec

The strain profiles were recorded using the LeCroy high-speed data acquisition system.

The Imacon-468-MK II digital CCD camera, manufactured by Hadland Photonics, was also used for these studies. The Imacon-468-MK II is capable of taking seven pictures at a framing rate of up to 100 million/second, with exposures as short as 10 nanoseconds. The camera was set to trigger off the incident strain pulse from the SHPB setup, send a flash command to a light unit, and begin taking a timed sequence of pictures at a given time from the initial signal. All the images were taken with an exposure time of 150ns unless otherwise stated. The versatility of the image timing allowed a series of real-time photographs to be taken from a single experiment, capturing different specimen strains.

The camera's imaging software is also capable of being calibrated from a known distance on an image in order to record measurements. A small plastic scale was attached to the transmitted bars near the specimen-bar interface, to facilitate calibration. This allowed the determination of specimen axial (length) as well as transverse (diametral) dimensions as a function of time during the dynamic loading process. The image analysis software of the camera was then utilized to determine the specimen axial and transverse strains.

4. Viscoelastic SHPB results

Results from the SHPB technique are valid only in the region where the specimen is in equilibrium. Thus, while analyzing the SHPB stress-strain plots, we should only concentrate on the time windows during which the specimen is in equilibrium. Low wave speeds in the test material made it necessary to use longer duration loading pulses to achieve equilibrium in the specimen. Bacon's method utilizes FFT analysis (of the strain signals), which is dependent on the sampling frequency and the sample size. Initial experiments done using Bacon's method under predicted the specimen strains due to the high sampling rate and long pulse durations. Thus, the 3-parameter Kelvin model developed by Fourney [12] was used for the viscoelastic SHPB data analysis. Four typical plots showing the complete SHPB analysis are given for polyurethane. These are the recorded strain profiles, the specimen true stress-strain plot, the true strain-time history and the specimen equilibrium plot. For the remaining materials only the engineering stress-strain plots are given.

4.1. Polyurethane results

Experiments were conducted on polyurethane EN-7 specimens in order to validate the experimental setup. The choice of this material was based on the available literature on soft material testing. Polyurethane is one of the softest materials, which has been tested using the conventional steel SHPB setup by various researchers [12, 14].

The total strain and strain rate achieved for the experiment shown in Fig. 4 was 20% and 1600/s respectively. The flow stress was 11 MPa. The plots show good equilibrium of the specimen at the time of maximum stress. Three experiments were conducted under identical conditions to check the repeatability of test results. The results for all the three tests matched very closely thus proving the repeatability of the technique.

Fig. 5 shows plots for the same material from an experiment conducted by Wilson [14], *et al*. The results of Fig. 4 compare well with the results from the earlier study by Wilson *et al*. Further, the viscoelastic bar setup resulted in a much cleaner transmitted pulse and better specimen equilibrium in comparison to the conventional SHPB setup used by Wilson *et al*. The specimen equilibrium was determined by measuring the stress at the incident and transmitted faces of the specimen, [5, 6]. A ratio of one between the incident and transmitted stresses would indicate specimen equilibrium. It was concluded that the viscoelastic SHPB setup and

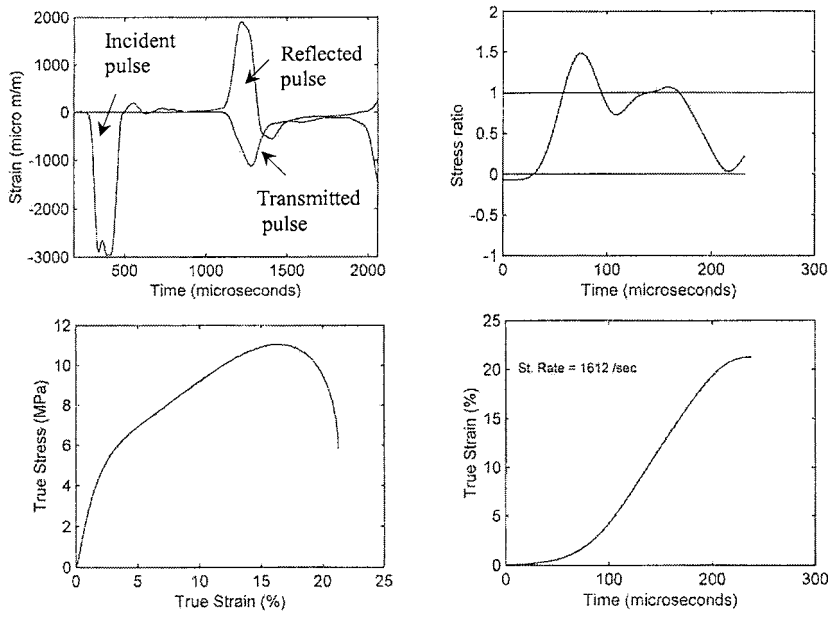

Figure 4 Polyurethane testing results using the viscoelastic SHPB setup showing the well defined transmitted pulse.

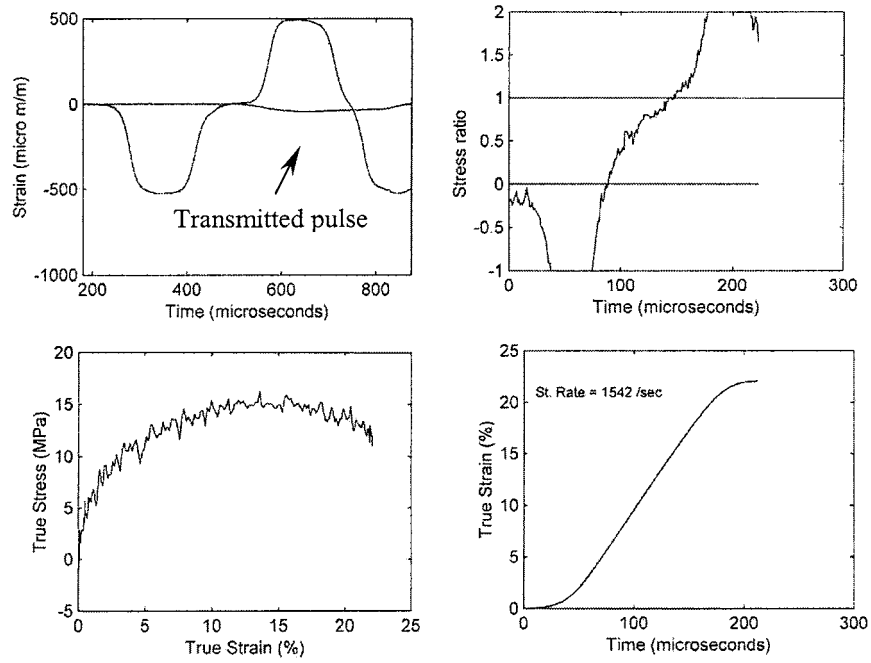

Figure 5 Experimental results for polyurethane testing using conventional SHPB setup, Wilson *et al.* Note: the small amplitude transmitted pulse.

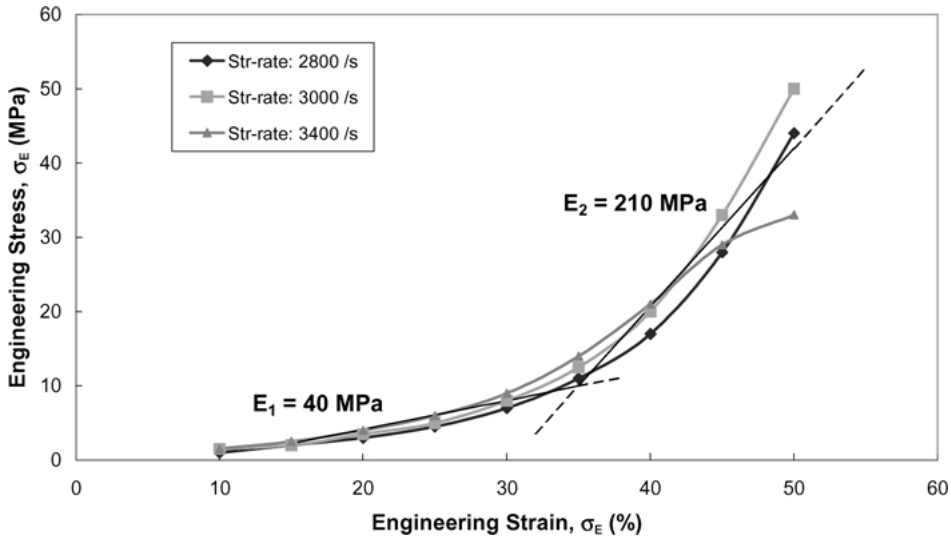

Figure 6 Engineering stress-strain plot for sorbothane showing the strain rate variation and 400% increase in stiffness at 35% strain.

data analysis developed were correct and better suited for low impedance material testing.

4.2. Sorbothane results

Sorbothane is a soft viscoelastic material, primarily used for shock absorption applications. The static strength reported by the manufacturer is 38 kPa at 44% strain, though it can undergo more than 250% compression. Fig. 6 shows the typical engineering stress-strain plots from the viscoelastic SHPB experiments. The plot shows the strain rate dependence of sorbothane within the tested strain rate range. An approximately 400% increase in sorbothane stiffness is observed after 35% strain, from 40 MPa to 210 MPa. The dynamic strength of sorbothane increased by about three orders of magnitude compared to the manufacturer specified static strength. For Sorbothane the maximum stress was achieved at a strain-rate of 3030/s. The maximum stress achieved was 50 MPa at 50% strain. The specimen reverted back to its original dimensions after the test.

4.3. Clay results

Fig. 7 shows typical engineering stress-strain results for clay, showing the strain-rate dependence within the tested strain-rate range. Clay also showed a 400% increase in stiffness after 30% strain, from 20 MPa to 90 MPa. The specimens were in good equilibrium at the time of maximum stress and strains.

The dynamic compressive strength of clay increased by four orders of magnitude compared to the static compressive strength (2 kPa) obtained using ASTM std. D695 [15]. This standard is used for determining the unconfined static compressive strength of cohesive soils. The static compressive strength for these

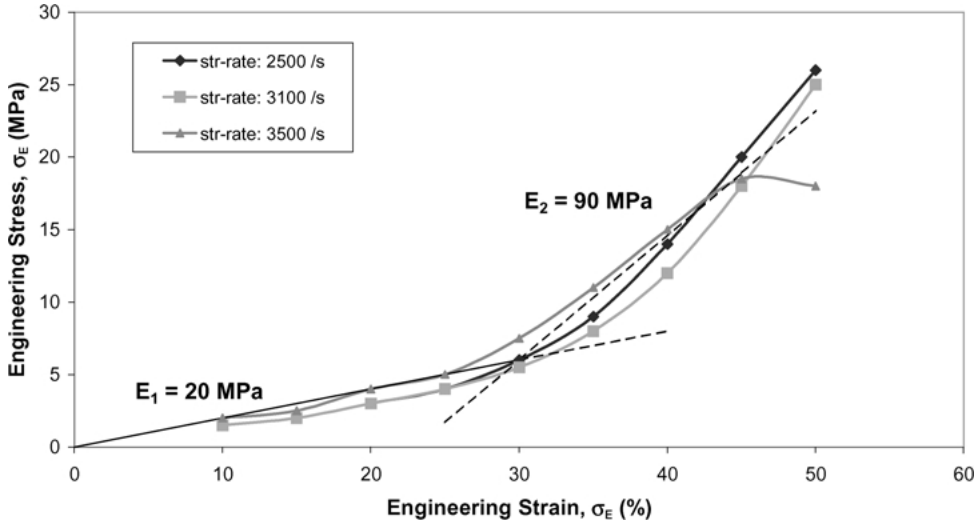

Figure 7 Engineering stress strain plot for clay showing strain-rate dependence with in the tested range.

materials is defined as the load at 15% strain. The maximum stress achieved was 30 MPa at ∼55% strain, for both 254 mm and 356 mm projectiles. The specimens were squashed at the end of the tests, making any post mortem analysis difficult.

4.4. Bologna results

Bologna was tested as an example of biological material. Knowledge of high strain rate behavior of biological tissues and human tissue in particular is crucial for numerical simulation studies of crash situations and behind armor injuries. Most of the existing literature on biological tissues deals with uni-axial tensile or shear loading [16]. In these experiments Bologna was subjected to dynamic compressive loads using the viscoelastic SHPB set up.

As with the other materials, three projectile lengths, (152, 254 and 356 mm) were used at an air gun firing pressure of 210 kPa. Three experiments were conducted for each projectile length. Fig. 8 shows typical stress-strain plots for bologna. The specimen was in good equilibrium at the instant of maximum stress and strains. The maximum stress achieved was 45 MPa at 60% strain and 3230/sec strain rate. Fig. 8 also shows the strain-rate dependence for bologna within the tested strain rates. The samples were squashed at the end of the test, making any post-mortem analysis impossible. Bologna also showed a 400% increase in stiffness after 35% strain, from 25 MPa to 125 MPa.

The experimental results show very high strain rate sensitivity for all the tested materials. The peak stresses for all the materials increased by more than 3 orders of magnitude for a 2 order of magnitude increase in rate of loadings. The SHPB setup cannot give another order of strain-rate increase. Further, all the tested materials showed a 5 times increase in the material stiffness at around 35% strain values. This increase in stiffness could be due to the non-linearity of these materials, which becomes more exemplified at high strain values. A look at the micro-mechanics of these materials is required to exactly understand this behavior.

5. Strain measurement using high-speed photography

High-speed photography in conjunction with the SHPB technique was used to obtain real-time specimen

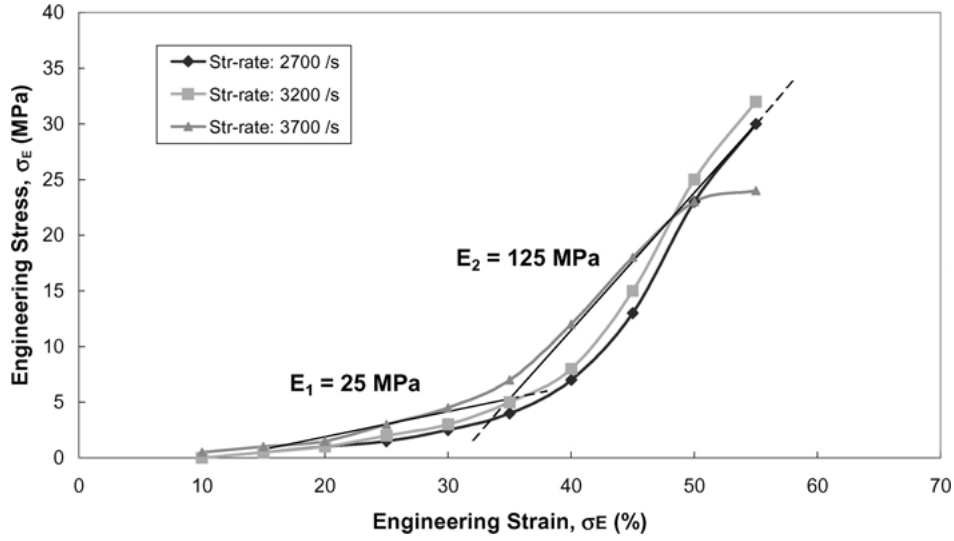

Figure 8 Engineering stress-strain plots for Bologna showing the strain rate effect and five times increase in stiffness.

axial and transverse strain information. Ramesh and Narasimhan [17] had developed an optical technique for measuring radial deformations of a specimen during split Hopkinson pressure bar testing. The high-speed photography technique used by us gives both the radial as well as the axial strain in real time. These experiments were conducted to verify the viscoelastic analysis model as well as to study the specimen strains under dynamic loading conditions.

Experiments were conducted on four different materials: brass, sorbothane, clay and polyurethane. The existing 12.7 mm SHPB facility at the Dynamic Photomechanics Laboratory, URI, was used for testing brass, while the viscoelastic SHPB setup developed during the course of this study was used for testing polyurethane, clay and sorbothane. The Imacon-468-MK II digital CCD camera was used for these studies.

The conventional SHPB theory is well established. Thus, the 12.7 mm steel SHPB setup and brass were chosen to validate the high-speed photography technique for measuring the axial and transverse strains. Care was taken to ensure that the camera lens was at the same horizontal and vertical level as the specimen, to obtain true specimen dimensions from the photographs.

5.1. Theoretical prediction of instantaneous diameter

Assuming the specimen material to be homogeneous, isotropic and incompressible i.e., the specimen density doesn't change the specimen diameter and thus the transverse strain at any instant can be found using mass conservation. Let the specimen initial and instantaneous diameter and lengths be d_0, d, l_0 and l respectively. Then from conservation of mass:

$$\frac{\pi}{4} l_0 d_0^2 \rho = \frac{\pi}{4} l d^2 \rho \tag{15}$$

where ρ is the specimen density.

$$\frac{l}{l_0} = \frac{d_0^2}{d^2} \Rightarrow \frac{l - l_0}{l_0} = \frac{d_0^2 - d^2}{d^2} \tag{16}$$

The engineering strain ε at any instant is defined as

$$\varepsilon = \frac{l - l_0}{l_0}$$

Thus,

$$d = \frac{d_0}{\sqrt{(1 + \varepsilon)}} \tag{17}$$

Therefore from the knowledge of specimen axial strain, we can predict the instantaneous diameters and transverse strains. The transverse engineering strain is defined as

$$\varepsilon_t = \frac{d - d_0}{d_0} \tag{18}$$

Instantaneous axial strains from the high-speed photography and the SHPB setup were compared and used to predict the instantaneous specimen diameters and transverse strains.

5.2. Experimental results

The transverse strains were measured for four different materials: brass, polyurethane, sorbothane and clay. Brass was tested using the existing 12.7 mm steel SHPB setup. A 356 mm steel projectile and 690 kPa air gun firing pressure was used for the experiment. The polyurethane sorbothane and clay specimens were tested using the viscoelastic SHPB setup developed as part of this study. A 356 mm PMMA projectile and 210 KPa firing pressure was used for all three experiments. A 105 mm Nikon lens along with a 11 mm extension tube was used for the high-speed camera with exposure times of 150 nanoseconds unless otherwise stated. The minimum resolution of the camera analysis software for this experimental set up was 0.08 mm/pixel.

5.2.1. Brass results

Seven photographs were taken with an inter-frame timing of 20 μseconds, Fig. 9. The specimen was a disc with diameter 10.16 mm and length 2.92 mm. The specimen final diameter and lengths were respectively 10.62 mm and 2.69 mm. The strain rate was 785/sec. Fig. 10 shows the SHPB results for the same experiment. The strain-rate for all the experiments was obtained from the slope of the linear part of the strain-time curve.

Table II gives a summary of the transverse and axial engineering strain calculations using both the high-speed camera and SHPB measurements. The axial strains obtained from high-speed photography are in very good agreement with the strains obtained by the SHPB technique. The maximum axial strain from

TABLE II Summary of transverse strains for brass SHPB testing

Frame no.	Time (μsec)	Diameter$_{inst.}$ (mm)	Diametral ε (%)	$L_{inst.}$ (mm)	Axial strain (%)		Transverse Str-ratio	
					Camera	SHPB	Camera	SHPB
1	0	10.16	0.00	2.95	0.0	0		
3	40	10.36	1.97	2.86	−3.1	−3.6	0.64	0.56
5	80	10.44	2.76	2.77	−6.1	−7.2	0.45	0.39
7	120	10.62	4.53	2.68	−9.2	−9.1	0.49	0.50

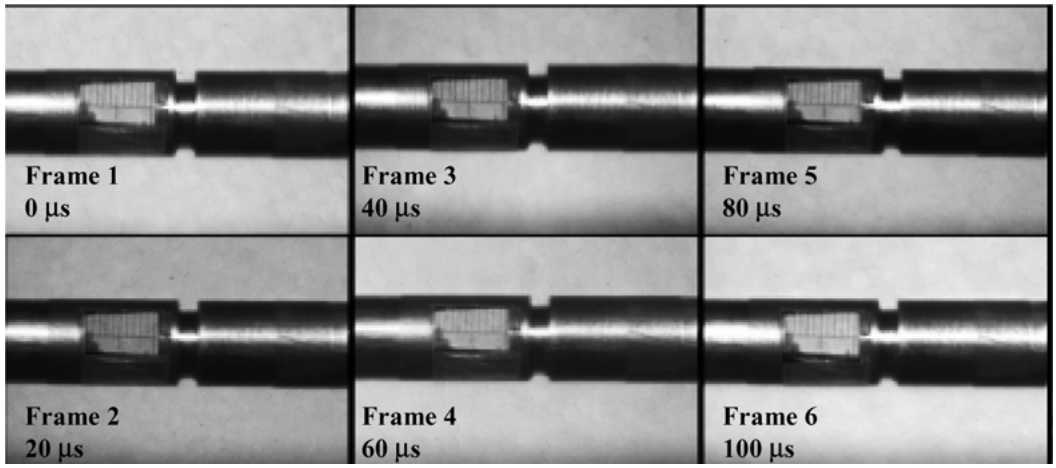

Figure 9 Photograph showing the brass specimen sandwiched between the two bars at different instants during the test.

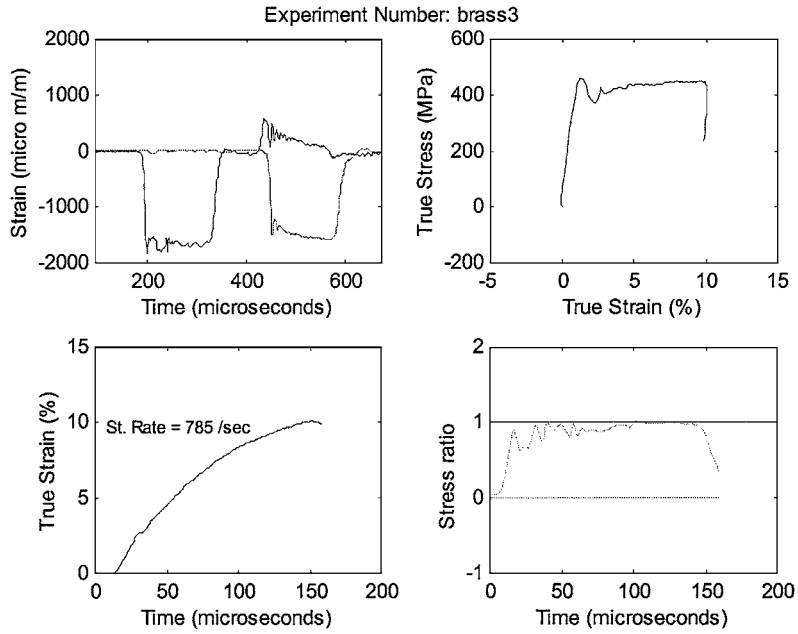

Figure 10 Plots showing the SHPB results for brass, using the 1/2 inch steel SHPB setup.

TABLE III Comparison of theoretically predicted and high-speed photographed instantaneous diameters for brass

Time (μsec)	Instantaneous diameter (mm)	
	Camera	Theoretical
0	10.16	10.16
40	10.36	10.32
80	10.44	10.48
120	10.62	10.65

both techniques is 9%. The errors in measurement of strain are within the range of the minimum resolution 0.08 mm of the camera imaging software. Table III compares the camera measured and theoretically predicted (Equation 17) values of the instantaneous specimen diameter. The axial strains obtained from the SHPB analysis were used in calculating the theoretical instantaneous diameters. The two values match within an error of 0.5%.

This experiment proved the feasibility of using high-speed photography for measuring specimen axial as well as transverse strains during dynamic loadings.

5.2.2. Sorbothane results

The inter-frame timings for sorbothane were 35 μseconds, with an exposure time of 120 nanoseconds. Fig. 11 shows 6 of the frames. Fig. 12 plots the axial engineering strains from both the SHPB analysis as well as from the high-speed camera. The axial strains measured from the SHPB setup are slightly less than the strains measured using the camera. The maximum axial strain measured using the camera is 66%, while the maximum axial strain from the SHPB analysis is 56%. The maximum transverse strain recorded using the camera is 73%.

The mismatch between the two axial strain measurements made it necessary to determine the more reliable

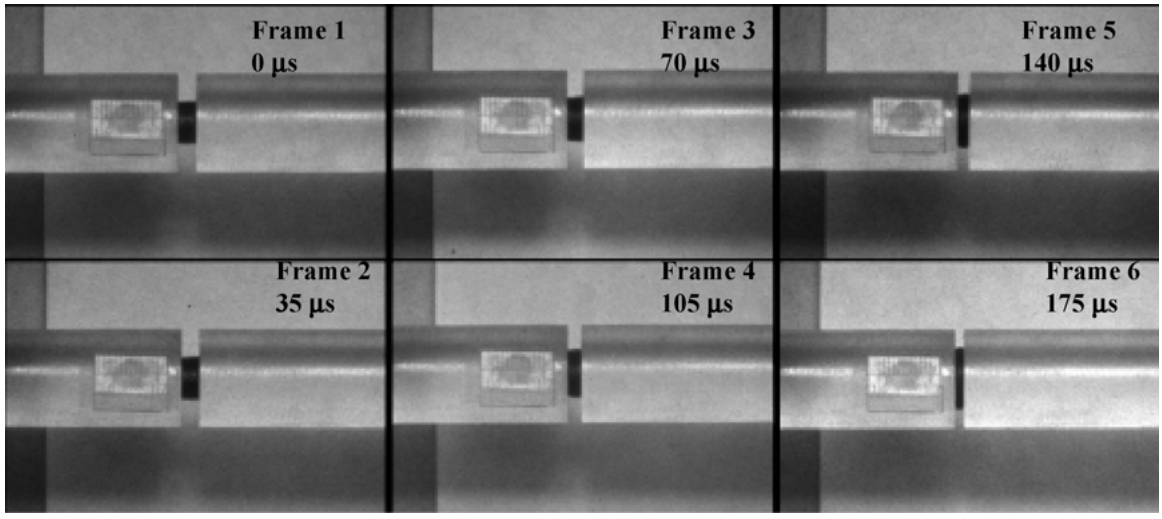

Figure 11 Photograph showing sorbothane specimen during dynamic compressive testing using the viscoelastic SHPB setup.

TABLE IV Comparison of theoretically predicted and high-speed photographed instantaneous diameters for sorbothane

Time (μsec)	Instantaneous diameter (mm)	
	Camera	Theoretical
0	8.0	8.0
70	8.4	8.3
105	9.0	9.1
140	10.0	9.8
175	11.5	11.5
210	13.8	13.8

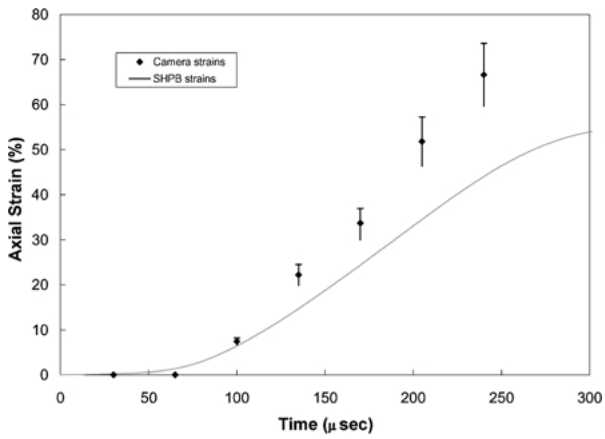

Figure 12 Plot comparing axial strains from the camera and viscoelastic SHPB analysis for sorbothane. The two techniques give similar strain-time profiles but significant differences in the strain values.

of the two measurement techniques. For validating the camera strain measurements, the measured instantaneous specimen diameters were compared with the theoretically predicted instantaneous diameters using Equation 17 and the camera measured axial strains, Table IV. The good match between the measured and predicted values, the two values match with in an error of 2%, indicated consistency within the two camera measurements making it more reliable of the two strain measuring techniques.

TABLE V Comparison of theoretically predicted and high-speed photographed instantaneous diameters for clay

Time (μsec)	Instantaneous diameter (mm)	
	Camera	Theoretical
0	9.5	9.5
70	10.2	10.6
105	11.5	11.4
140	13.2	12.6
175	16.0	15.4
210	18.8	17.2

TABLE VI Polyurethane measured and predicted instantaneous diameters

Time (μsec)	Instantaneous diameter (mm)	
	Camera	Theoretical
0	8.75	8.75
70	9.13	9.3
105	9.75	10.2
140	10.5	10.8
175	11.5	11.9
210	12.25	12.36

5.2.3. Clay results

The inter-frame timings for clay were 35 μseconds, with exposure times of 100 nanoseconds. Fig. 13 shows 6 of the frames captured using the Imacon-468-Mk II camera. Fig. 14 shows a comparison of the strains obtained from the camera and the SHPB analysis for this experiment. The axial strains obtained from the SHPB analysis are around 20% lower than the strains measured using the camera. Table V gives a comparison of the measured and predicted (Equation 17) instantaneous diameters. The two values match within an error of 8%.

5.2.4. Polyurethane results

The inter-frame timings for polyurethane were 35 μseconds, with an exposure time of 120 nanoseconds.

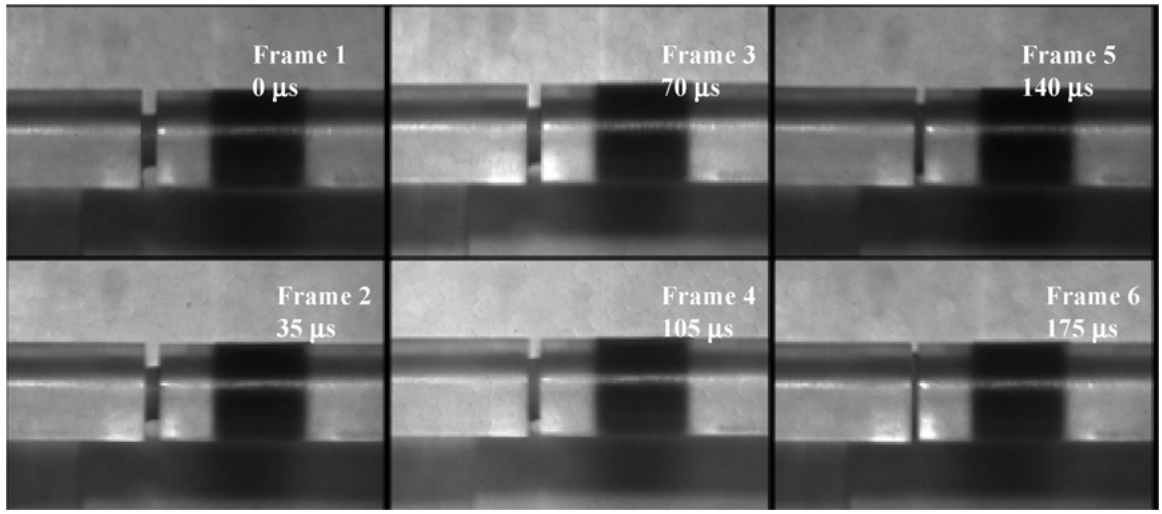

Figure 13 Photograph showing viscoelastic SHPB testing of clay.

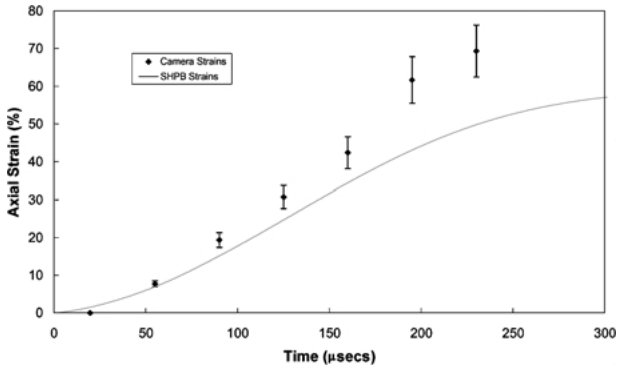

Figure 14 Comparison of viscoelastic SHPB and camera axial strains for clay.

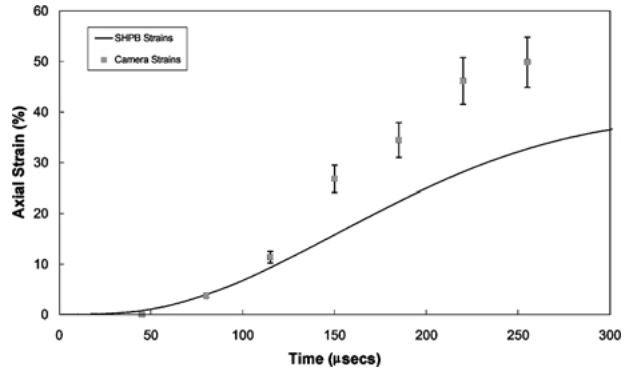

Figure 16 Plot of axial strains from the camera and SHPB analysis for polyurethane.

Fig. 15 shows 6 of the frames. Fig. 16 compares the camera and SHPB axial engineering strains. The axial strains measured from the SHPB setup are less than the strains measured using the camera. The maximum axial strain measured using the camera is 50%, while the maximum axial strain from the SHPB analysis is 40%. The maximum transverse strain recorded using the camera is 40%. Table VI shows a good match between the measured and predicted (Equation 17) values of the instantaneous specimen diameter.

6. Conclusions

The dynamic strengths of three compliant materials sorbothane, clay and bologna were determined using a viscoelastic SHPB setup. Also, experiments conducted

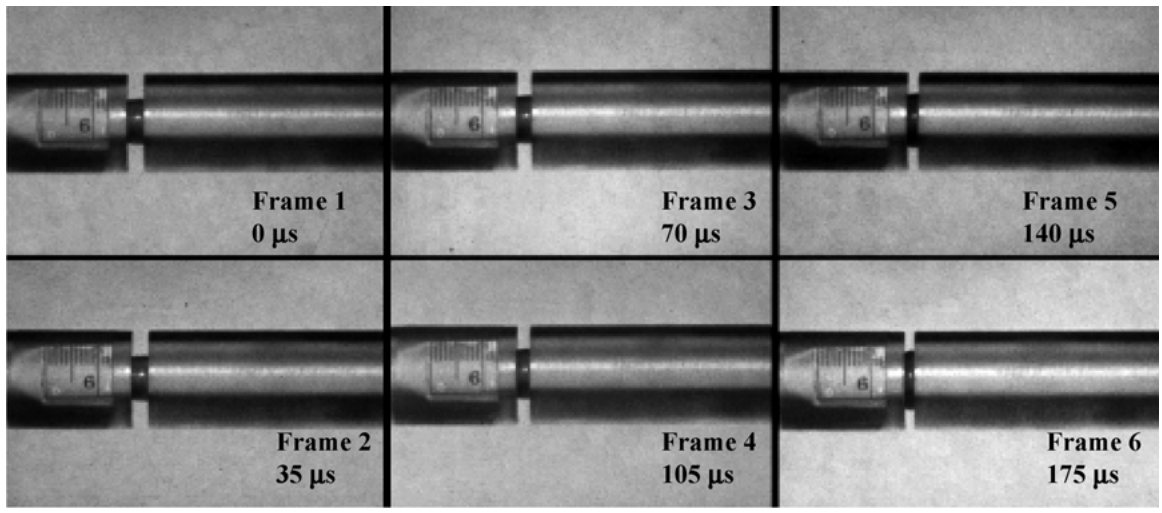

Figure 15 Photograph showing polyurethane specimen during dynamic SHPB testing.

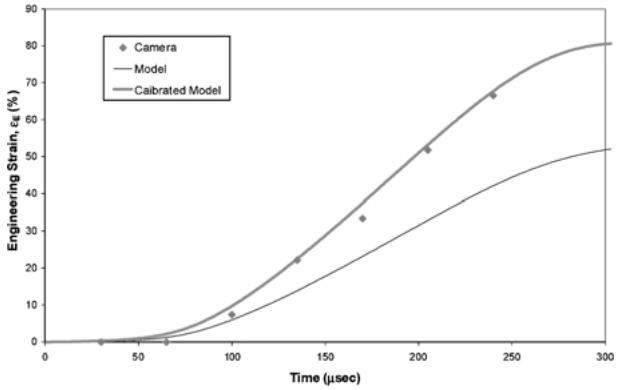

(a)

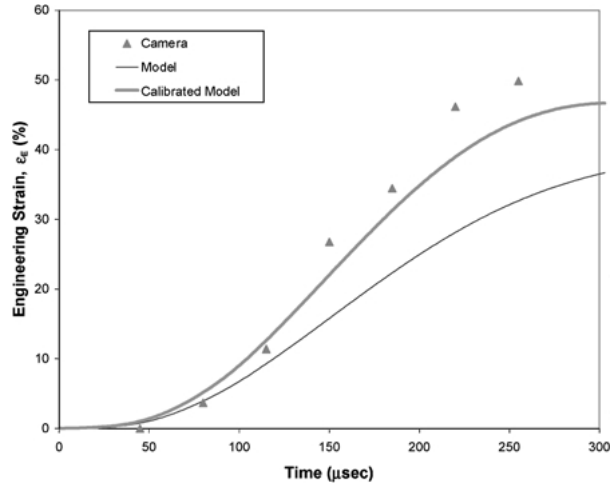

(b)

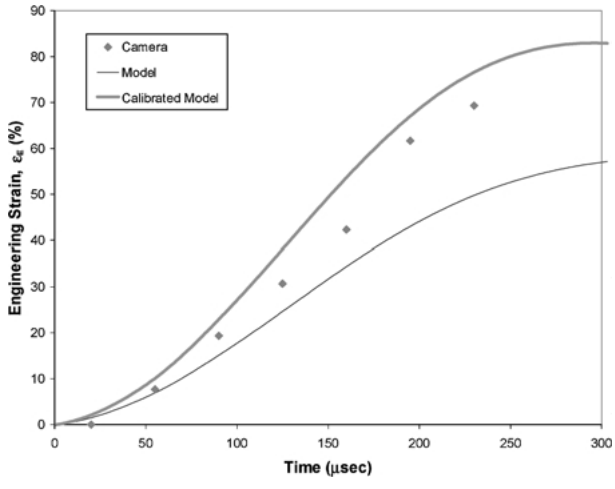

(c)

Figure 17 Comparison of axial strains obtained from the camera, model and recalibrated model analysis for (a) sorbothane, (b) polyurethane and (c) clay.

using the SHPB set up in conjunction with high-speed photography allowed the measurement of both axial as well as diametric strains under dynamic loadings. There was a good match of the instantaneous diameter measurements obtained from the camera and the predicted instantaneous diameters based on volume conservation and the specimen material incompressibility.

All three tested materials: Clay, Sorbothane and Bologna showed very high strain-rate dependence. The dynamic compressive strength of clay increased by 4 orders of magnitude compared to its static compressive strength, 2 kPa. The maximum stress achieved in clay was 30 MPa at 50% strain and 3100/s strain-rate. For sorbothane the maximum stress obtained was 50 MPa at 50% strain at a strain-rate of 3000/sec. There was a 3 orders of magnitude increase in the dynamic compressive strength of sorbothane compared to the manufacturer specified static value of 38 KPa. For bologna the static compressive strength was too small to be measured accurately while the maximum stress obtained was 45 MPa at 60% strain and strain-rate of 3200/s. All the tested materials showed a 400% increase in stiffness after 30% strain.

The feasibility of using high-speed photography for measuring dynamic axial and transverse strains was validated. There was less than 2% difference between the axial strains measured using the conventional steel SHPB and the high-speed camera. Also the camera measured instantaneous specimen diameters matched very well with the theoretically predicted instantaneous dimensions. The camera measured instantaneous diameters also matched very well with the theoretically predicted instantaneous diameters for clay, polyurethane and sorbothane. The axial strains obtained using the viscoelastic bars for all the tested materials were about 15% lower than the axial strains obtained using the high-speed camera. This may possibly be due to the various assumptions made in the theoretical modeling of the viscoelastic bars. At this point it must be mentioned that of all the viscoelastic models discussed earlier, Fourney's [10] model gave the best match with the high-speed camera experiments.

Using the results from the high-speed photography experiments the viscoelastic bars were recalibrated. It was observed that the viscoelastic model's predictions of specimen axial strain improved for all three materials if the bar material properties were changed so as to stiffen the bars. The material constants of the 3 parameter Kelvin model for the empirically recalibrated bars were $E_0 = 3.88$ GPa, $E_1 = 132.27$ GPa and $\theta_1 = .0012$ sec. The predicted axial strains using these material constants are shown in Fig. 17 for the three materials. There was a very good match between the high-speed photography axial strains and the strains predicted by the recalibrated viscoelastic model for sorbothane. The model over predicted the axial strains by an average of 5% for polyurethane and under predicted the axial strains by an average of 5% for clay. The deviation of $\pm 5\%$ is within the experimental error for measurements.

Acknowledgments

The authors would like to acknowledge the support of NSF under grant No. CMS9870947.

References

1. S. J. BELL, Structural Materials Center Report 325–331, DRA Holton Health, UK. (1996).
2. G. J. COOPER, *Journal of Biomechanics* **24**(5) (1991) 273.
3. H. KOLSKY, "Stress Waves in Solids" (Dover Publications, New York, 1963).
4. E. DAVIES and S. C. HUNTER, *Journal of Mechanics and Physics of Solids* **11** (1963) 155.

5. G. T. GRAY and W. R. BLUMENTHAL, 2000, in "ASM Handbook, Vol. 8: Mechanical Testing and Evaluation" (ASM International, 2000) p. 488.
6. G. T. GRAY, W. R. BLUMENTHAL, C. P. TRUJILLO and R. W. CARPENTER, *Journal De Physique IV, France, Colloq. C3* **7** (1997) 523.
7. M. J. FORRESTAL, W. CHEN and B. ZHANG, *Experimental Mechanics* **39**(2) (1999).
8. L. WANG, K. LABIBES, Z. AZARI and G. PLUVINAGE, *International Journal of Impact Mechanics* **15** (1994) 669.
9. H. ZHAO, G. GARY and J. R. KLEPACZKO, *ibid.* **19** (1997) 319.
10. O. SAWAS, N. S. BRAR and R. A. BROCKMAN, *Experimental Mechanics* **38**(2) (1998).
11. C. BACON, *ibid.* **38**(4) (1998).
12. W. L. FOURNEY, private communication.
13. K. F. GRAFF, "Wave Motion in Elastic Solids" (Dover Publications, New York, 1975).
14. J. WILSON, Master's Thesis, University of Rhode Island, Kingston, RI, 2000.
15. Standard Test Method for Unconfined Compressive Strength of Cohesive Soil, American Society for Testing and Materials (ASTM) D695, 1996.
16. Y. C. FUNG, "Biomechanics Mechanical Properties of Living Tissues" (Springer-Verlag, New York, 1984).
17. K. T. RAMESH and S. NARSIMHAN, *International Journal of Solids and Structures* **33** (1996) 3723.

Received 12 October 2000
and accepted 22 October 2001